ENHANCED MODEL PREDICTIVE CURRENT CONTROL FOR ELIMINATING ZERO-SEQUENCE VOLTAGE AND REDUCING CURRENT HARMONICS IN NINE-SWITCH INVERTER FED OPEN-END LOADS

Vu Huu Cong[1], Tran Quoc Hoan[2]*

[1]*Hanoi University of Civil Engineering, Hanoi, Vietnam*

[2]*Tran Dai Nghia University, Ho Chi Minh City, Vietnam*

*Email: *hoantq@tdnu.edu.vn*

Received: 4 February 2025; Revised: 5 March 2025; Accepted: 14 March 2025

ABSTRACT

This paper presents an enhanced model predictive current control (MPCC) strategy designed to eliminate zero-sequence voltage (ZSV) and reduce current harmonics in nine-switch inverter (NSI) systems driving open-end loads. The proposed approach begins by formulating a control set comprising seven voltage vectors that inherently produce zero ZSV, ensuring effective ZSV elimination. Within each sample period, three of these voltage vectors are ideally used to further improve output current performance. Simulations utilizing PSIM software are used to verify the effectiveness of the proposed method.

Keywords: Model predictive current control (MPCC), nine-switch inverter (NSI), zero-sequence voltage (ZSV), current harmonics.

1. INTRODUCTION

Three-level inverters have several important advantages over traditional two-level inverters, such as a lower dv/dt, less switching stress, less total harmonic distortion (THD), a smaller filter size, and less electromagnetic interference (EMI) [1]. These benefits have driven the widespread adoption of three-level inverters in various industrial applications, including motor drives, power quality improvement, electric vehicles, uninterruptible power supplies, and wind energy systems [2-3]. The three-level neutral-point-clamped inverter (3L-NPC), the three-level flying-capacitor inverter (3L-FC), the three-level T-type inverter (3L-T type), and the dual two-level inverter with an open-end load are some of the most well-known three-level inverter topologies [4-7].

Among these, the dual-inverter topology (Figure 1) stands out due to its enhanced DC voltage utilization, increased modulation flexibility, and straightforward fault-tolerant operation [8]. However, like other three-level inverters such as 3L-NPC, 3L-FC, and 3L-T type inverters, the dual-inverter topology requires 12 active switches, leading to increased complexity and cost. To address this limitation, Z. Yu et al. [9] introduced the nine-switch inverter (NSI) for open-end loads (Figure 2), which reduces the number of active switches to nine, simplifying control circuitry and lowering system costs.

Like the dual two-level inverter system driven by a single DC source, zero-sequence voltage (ZSV) has an impact on the NSI for open-end loads. The presence of ZSV leads to zero-sequence currents (ZSC), resulting in increased power losses and distorted output currents [10]. Thus, eliminating the ZSV component is critical for improving the performance and efficiency of NSI systems.

Model predictive current control (MPCC) has recently emerged as an effective and straightforward strategy for controlling voltage source inverters (VSIs) [11-12]. MPCC operates by using the system's discrete-time model to predict output currents for all possible voltage vectors. It selects the optimal vector by minimizing a predefined cost function, ensuring superior current control. This approach has been successfully applied to various three-level VSIs, including the three-phase 3L-NPC inverter [13], the three-phase 3L-T type inverter [14-15], and the five-phase three-level inverter

[16]. The popularity of MPCC is a result of its theoretically straightforward implementation, robust handling of nonlinearities and constraints, and quick dynamic responsiveness.

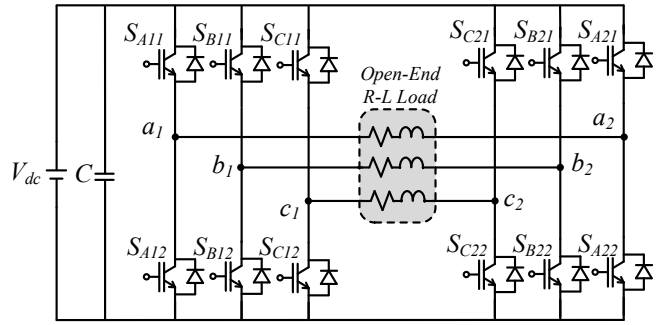

Figure 1. Dual two-level inverter fed open-end load

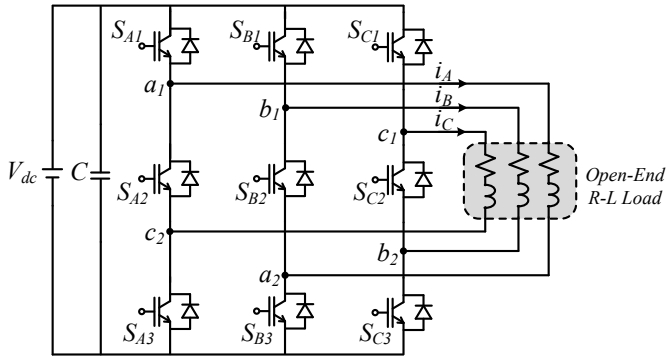

Figure 2. Nine-switch inverter fed open-end load

Despite its advantages, the application of MPCC for controlling NSIs with open-end loads remains unexplored in existing literature. Moreover, conventional MPCC methods [17] cannot simultaneously achieve reduced output current ripple and ZSV elimination, highlighting a key limitation.

To address these challenges, this paper proposes an enhanced MPCC approach for NSIs supplying open-end loads. The primary objectives are to eliminate ZSV components and reduce harmonic currents. The proposed method begins by devising a control set of seven voltage vectors, each characterized by zero ZSV. A reference voltage vector is then introduced to eliminate the need for current prediction calculations. Additionally, three voltage vectors are employed within each sampling period to enhance output current performance.

Table 1. Switching states of each leg of the NSI

Switching State	S_{X1} (X=A,B,C)	S_{X2} (X=A,B,C)	S_{X3} (X=A,B,C)	U_{mO} (m=a_1,b_1,c_1)	U_{nO} (n=a_2,b_2,c_2)
2	1	1	0	V_{dc}	V_{dc}
1	1	0	1	V_{dc}	0
0	0	1	1	0	0

2. CONVENTIONAL MPCC FOR NSI FED OPEN-END LOAD

2.1. Circuit structure

Figure 2 illustrates the power circuit of the NSI supplying a three-phase open-end load. This topology comprises three inverter legs powered by a dc-link voltage V_{dc}. As shown, each phase of the load is connected to the upper and lower terminals of two separate inverter legs, providing flexibility in voltage generation.

Each inverter leg incorporates three switches, whose operation adheres to two critical switching constraints [9]:

1. All three switches in a single leg cannot be simultaneously active, preventing short circuits across the DC bus.

2. At least two switches in the same leg must remain active to maintain continuous current flow through the inductive load.

These constraints result in three permissible switching states for each leg, enabling safe and efficient operation, as summarized in Table 1. Compliance with these constraints results in three permissible switching states for each leg, facilitating safe and efficient operation, as shown in Table 1. Consequently, the NSI can produce three levels of output voltage $\left(V_{dc}, 0, -V_{dc}\right)$ based on its switching states. The phase voltages $\left(U_a, U_b, U_c\right)$ of the NSI are determined by the following equation:

$$\begin{aligned} U_a &= U_{a_1a_2} = U_{a_1O} - U_{b_2O} \\ U_b &= U_{b_1b_2} = U_{b_1O} - U_{c_2O} \\ U_c &= U_{c_1c_2} = U_{c_1O} - U_{a_2O} \end{aligned} \qquad (1)$$

Each leg of the NSI can operate in three distinct switching states, leading to a total of 27 possible switching combinations. Each combination corresponds to a specific voltage vector, which is transformed into the $\alpha\beta$ coordinate frame using the Clarke transformation [8]:

$$\mathbf{V} = \left(U_a + e^{j2\pi/3}U_b + e^{j4\pi/3}U_c\right) \qquad (2)$$

The 27 voltage vectors are categorized into four groups based on their magnitudes: zero vectors, small vectors, middle vectors, and large vectors, as illustrated in Figure 3. The corresponding ZSV components U_{ZSV} for these vectors are calculated using the equation:

$$V_{ZSV} = \frac{U_a + U_b + U_c}{3} \qquad (3)$$

Details are presented in Table 2. The inherent ZSV component generated by the NSI results in a ZSC i_{ZSC}, as expressed by:

Table 2. Voltage vectors of the NSI fed open-end load

Voltage Vector		Switching State			Magnitude of $V_{\alpha\beta}$	V_{zsv}	Voltage Vector		Switching State			Magnitude of $V_{\alpha\beta}$	V_{zsv}
		Leg a	Leg b	Leg c					Leg a	Leg b	Leg c		
Zero Vector	V_0	0	0	0	0	0	Small Vector	V_1	0	0	1	$\frac{2V_{dc}}{3}$	$\frac{V_{dc}}{3}$
	V_{26}	2	2	2				V_3	0	1	0		
	V_{13}	1	1	1		V_{dc}		V_5	0	1	2		
Middle Vector	V_2	0	0	2	$\frac{2V_{dc}}{\sqrt{3}}$	0		V_9	1	0	0		
	V_6	0	2	0				V_{15}	1	2	0		
	V_8	0	2	2				V_{17}	1	2	2		
	V_{18}	2	0	0				V_{19}	2	0	1		
	V_{20}	2	0	2				V_{23}	2	1	2		
	V_{24}	2	2	0				V_{25}	2	2	1		
Large Vector	V_7	0	2	1	$\frac{4V_{dc}}{3}$	$\frac{V_{dc}}{3}$		V_4	0	1	1		$\frac{2V_{dc}}{3}$
	V_{11}	1	0	2				V_{10}	1	0	1		
	V_{21}	2	1	0				V_{12}	1	1	0		
								V_{14}	1	1	2		
								V_{16}	1	2	1		
								V_{22}	2	1	1		

$$i_{ZSC} = \frac{i_a + i_b + i_c}{3} \tag{4}$$

where i_a, i_b, and i_c denote the output currents of phases a, b, and c, respectively.

The presence of i_{ZSC} introduces additional power losses and distorts the output currents [10]. Consequently, eliminating ZSV is crucial for improving system performance and efficiency.

2.2. Conventional model predictive current control

Figure 4 illustrates the block diagram of the conventional MPCC approach for an NSI supplying an open-end R-L load. For analytical simplicity, the load is modelled as an R-L circuit, as this can be readily extended to motor control applications [10, 14].

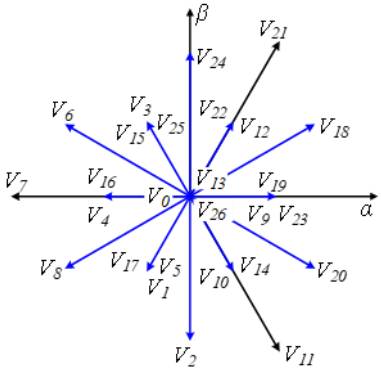

Figure 3. Space vector diagram of NSI fed open-end load

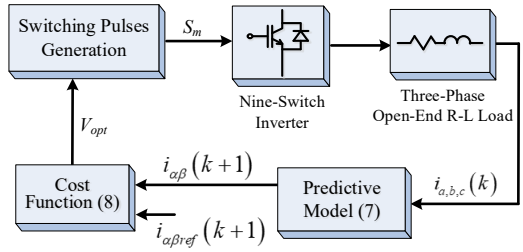

Figure 4. Block diagram of conventional MPCC method

Using Kirchhoff's voltage law, the continuous-time model of the NSI fed open-end R-L load is described as:

$$U_i = Ri_i + L\frac{di_i}{dt}, i = (a,b,c) \tag{5}$$

where L and R represent the load inductance and resistance, respectively. The Clarke transformation reformulates the model in the $\alpha\beta$ reference frame as:

$$\begin{aligned} U_\alpha &= Ri_\alpha + L\frac{di_\alpha}{dt} \\ U_\beta &= Ri_\beta + L\frac{di_\beta}{dt} \end{aligned} \tag{6}$$

By applying the forward Euler approximation method with a sampling time of T_s, the discrete-time model is obtained as:

$$\begin{aligned} i_a(k+1) &= \left(1 - \frac{RT_s}{L}\right) i_a(k) + \frac{T_s}{L} U_a(k) \\ i_b(k+1) &= \left(1 - \frac{RT_s}{L}\right) i_b(k) + \frac{T_s}{L} U_b(k) \end{aligned} \tag{7}$$

The objective of the conventional MPCC is to ensure that the output currents closely follow the reference current. To achieve this, a cost function is defined as:

$$g = \left(i_\alpha(k+1) - i_{\alpha ref}(k+1)\right)^2 + \left(i_\beta(k+1) - i_{\beta ref}(k+1)\right)^2 \tag{8}$$

The best voltage vector that minimizes the cost function is identified and used during each sample interval. This ensures minimal current errors and effective operation of the NSI.

3. PROPOSED MPCC FOR NSI FED OPEN-END LOAD

The conventional MPCC method, which employs a single voltage vector for controlling the NSI, is limited in its ability to simultaneously eliminate the ZSV component and reduce harmonic currents. To address these shortcomings, this paper presents an enhanced MPCC strategy specifically designed for an NSI supplying an open-end load. The primary goals are: i) eliminate the ZSV component, and ii) minimize harmonic currents.

The proposed strategy introduces a control set comprising seven voltage vectors, each ensuring a zero ZSV component, and employs three voltage vectors during each sampling period to improve output current performance.

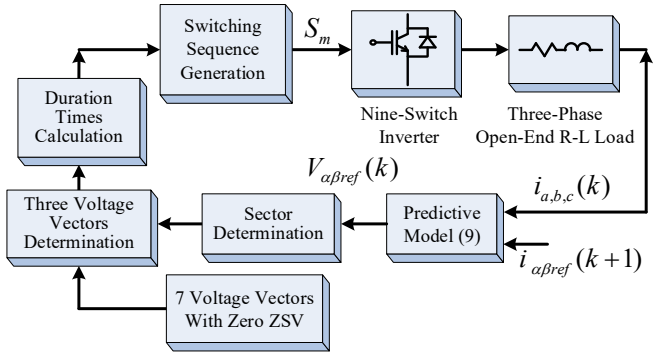

Figure 5. Block diagram of proposed MPCC method

The block diagram of the proposed method is presented in Figure 5. The implementation procedure of the proposed method can be summarized as follows:

Step 1: Measure the output currents i_a, i_b, and i_c, and determine the reference output currents $i_{\alpha ref}$, $i_{\beta ref}$.

Step 2: Compute the reference voltage vector using Equation (9) and determine its corresponding location.

Step 3: Select three voltage vectors from the set of seven voltage vectors with a ZSV component based on the location of the reference voltage vector.

Step 4: Calculate the duration times of the three selected voltage vectors using Equations (10), (11), and (12).

Step 5: Generate the appropriate switching sequence to control the NSI.

Table 3. Selected three voltage vectors according to sector

Sector	Voltage Vector	Sector	Voltage Vector
1	$V_0(000)$ $V_{18}(200)$ $V_{20}(202)$	4	$V_0(000)$ $V_6(020)$ $V_8(022)$
2	$V_0(000)$ $V_{18}(200)$ $V_{24}(220)$	5	$V_0(000)$ $V_2(002)$ $V_8(022)$
3	$V_0(000)$ $V_6(020)$ $V_{24}(220)$	6	$V_0(000)$ $V_2(002)$ $V_{20}(202)$

To eliminate the requirement for current prediction calculations, a reference voltage vector is derived directly from the discrete-time model of the system as:

$$\begin{aligned} V_{\alpha ref}(k) &= \frac{L}{T_s} i_{\alpha ref}(k+1) + \frac{RT_s - L}{T_s} i_\alpha(k) \\ V_{\beta ref}(k) &= \frac{L}{T_s} i_{\beta ref}(k+1) + \frac{RT_s - L}{T_s} i_\beta(k) \end{aligned} \tag{9}$$

The proposed method selects three voltage vectors closest to the reference voltage vector in the $\alpha\beta$-frame to enhance current performance while maintaining a zero ZSV component. These vectors are determined based on the reference voltage vector's sector, as illustrated in Figure 6 and outlined in Table 3.

A novel cost function is formulated to calculate the execution time for each voltage vector. For a selected voltage vector V_i, the cost function is given by:

$$g_{new} = \left|V_{\alpha ref}(k) - V_\alpha(k)\right| + \left|V_{\beta ref}(k) - V_\beta(k)\right| \tag{10}$$

For example, in Sector 2, the selected vectors are V_{18}, V_{24}, and V_0. The cost function values associated with these voltage vectors, g_{18}, g_{24}, and g_0, are defined as Equation (11):

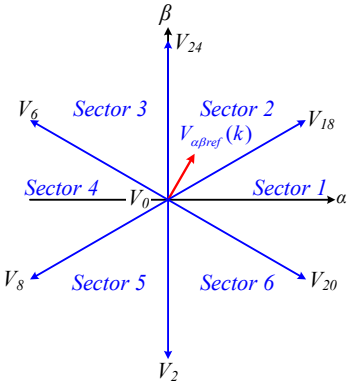

Figure 6. Selected voltage vectors of the proposed MPCC method

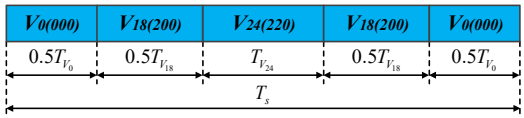

Figure 7. Generated switching sequence in sector 2 with the proposed MPCC method

$$\begin{cases} g_{18} = \left|V_{\alpha ref}(k) - V_{18\alpha}\right| + \left|V_{\beta ref}(k) - U_{18\beta}\right| \\ g_{24} = \left|V_{\alpha ref}(k) - V_{24\alpha}\right| + \left|V_{\beta ref}(k) - U_{24\beta}\right| \\ g_0 = \left|V_{\alpha ref}(k) - V_{0\alpha}\right| + \left|V_{\beta ref}(k) - U_{0\beta}\right| \end{cases} \tag{11}$$

Each voltage vector's execution time is inversely proportional to the value of its cost function, as shown:

$$\begin{cases} t_{V_{18}} = \dfrac{t_{V_0} t_{V_{24}} T_s}{t_{V_{18}} t_{V_{24}} + t_{V_0} t_{V_{24}} + t_{V_0} t_{V_{18}}} \\ t_{V_{24}} = \dfrac{t_{V_0} t_{V_{18}} T_s}{t_{V_{18}} t_{V_{24}} + t_{V_0} t_{V_{24}} + t_{V_0} t_{V_{18}}} \\ t_{V_0} = \dfrac{t_{V_{18}} t_{V_{24}} T_s}{t_{V_{18}} t_{V_{24}} + t_{V_0} t_{V_{24}} + t_{V_0} t_{V_{18}}} \end{cases} \tag{12}$$

To control the NSI, a switching sequence is created once the three voltage vectors and their corresponding execution times have been established. Figure 7 illustrates the switching sequence for Sector 2 under the proposed MPCC method.

By integrating a reference voltage vector approach, voltage vector selection based on proximity in the $\alpha\beta$-frame, and optimized execution times, the proposed MPCC strategy significantly improves current performance and eliminates the ZSV component.

4. SIMULATION AND RESULTS

To validate the performance of the proposed MPCC method, simulations were conducted using PSIM software. The simulation parameters were as follows: dc-link voltage V_{dc} = 100V; resistive load R = 13Ω; inductive load L = 15mH; output frequency reference f_{ref} = 50Hz. A comparative analysis was carried out among three MPCC methods:

1. Method I: Conventional MPCC without considering ZSV components.
2. Method II: Conventional MPCC designed to eliminate ZSV components.
3. Method III: Proposed MPCC method.

The results are presented in Figures 8, 9, and 10, with dynamic performance comparisons in Figure 11.

Figure 8 illustrates the steady-state performance of Method I. The output phase current i_a shows significant distortion. The ZSV component V_{ZSV} remains non-zero due to the inclusion of voltage vectors (V_1, V_3, V_9) with non-zero ZSV components in the control set. A prominent zero-sequence current i_{ZSC} is observed, resulting in additional power losses and degraded system performance.

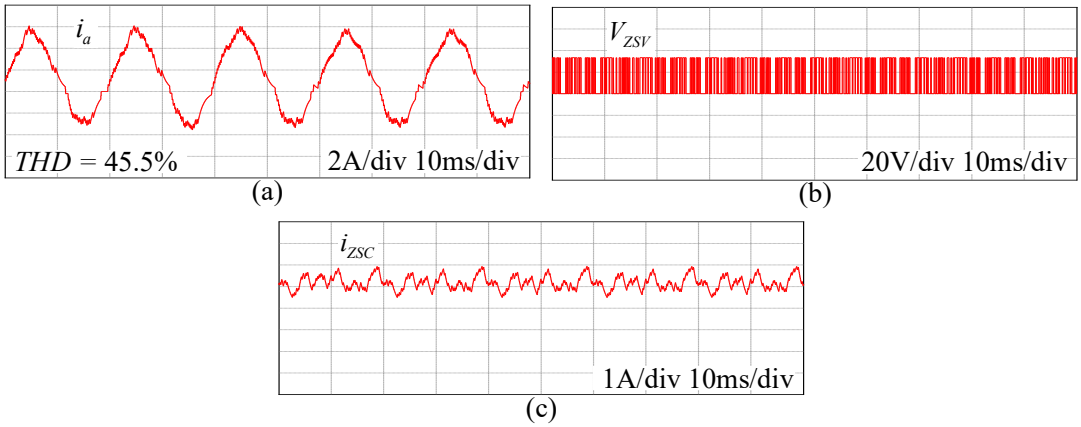

Figure 8. Simulated results of Method I: a) Output phase current i_a, b) ZSV component V_{ZSV}, and c) ZSC component i_{ZSC}

Figure 9 presents the steady-state waveforms for Method II. The output phase current i_a exhibits significant ripples. The ZSV component V_{ZSV} successfully eliminated by using only voltage vectors with zero ZSV. The zero-sequence current i_{ZSC} effectively eliminated. Despite its ability to eliminate V_{ZSV} and i_{ZSC}, Method II suffers from high output current ripple due to the use of a single voltage vector throughout the entire sampling period.

Figure 10 illustrates the steady-state performance of Method III. The output phase current i_a demonstrates reduced ripple compared to Method II, resulting in a smoother waveform. The ZSV component V_{ZSV} completely eliminated by employing three voltage vectors with zero ZSV per sampling period. The zero-sequence current i_{ZSC} eliminated effectively. The proposed method achieves superior performance by reducing harmonic distortion and mitigating ripple in the output current, underscoring its advantages over Method II.

Figure 11 shows the dynamic response of three MPCC methods during a step change in the output current reference from 2.5 A to 4.5 A. As observed in Figure 11, all three methods exhibit comparable responses to the current reference variation. However, the proposed MPCC method demonstrates superior output current quality compared to the other approaches studied. Specifically, as shown in Figure 11(a), Method I results in significant output current distortion due to the use of voltage vectors containing a non-zero ZSV component as the input control set. In contrast, the proposed method

achieves a sinusoidal output current with reduced ripple relative to Method II, which can be attributed to its utilization of three voltage vectors with a zero ZSV component within each sampling period.

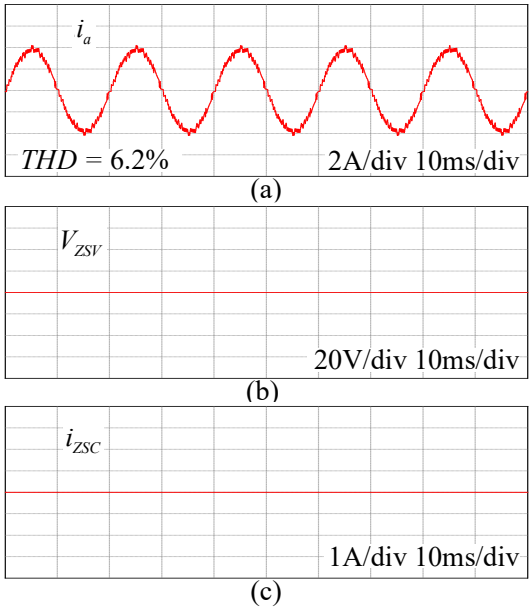

Figure 9. Simulated results of Method II: a) Output phase current i_a, b) ZSV component V_{ZSV}, and c) ZSC component i_{ZSC}

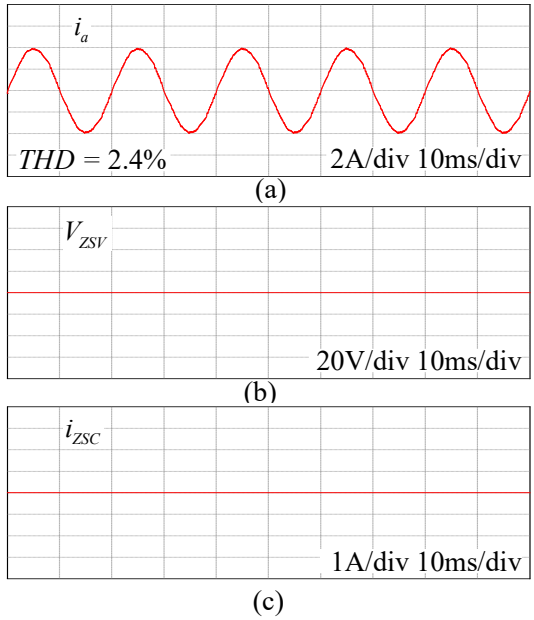

Figure 10. Simulated results of Method III: a) Output phase current i_a, b) ZSV component V_{ZSV}, and c) ZSC component i_{ZSC}

To assess the impact of model parameter mismatches on the performance of the proposed control method, a series of simulation tests were conducted, considering variations in load resistance and inductance. Specifically, five cases were examined to evaluate the effects of these mismatches:

Case 1: Accurate R and accurate L.

Case 2: 85% of accurate R and accurate L.

Case 3: 115% of accurate R and accurate L.

Case 4: Accurate R and 85% of accurate L.

Case 5: Accurate R and 115% of accurate L.

As shown in Figure 12, the THD performance across these five cases exhibits minimal variation with respect to changes in load resistance and inductance. These results indicate that the proposed control scheme effectively mitigates the adverse effects of model parameter mismatches.

The simulation results validate the effectiveness of the proposed MPCC method. By leveraging three voltage vectors with zero ZSV in each sampling period, the proposed method eliminates V_{ZSV} and i_{ZSC}, reduces output current ripple, and improves THD compared to conventional methods. Moreover, its dynamic performance is on par with the conventional approach, further demonstrating its practical advantages.

5. CONCLUSION

This paper presented an enhanced MPCC strategy designed to eliminate the ZSV component and improve output current performance in a NSI driving an open-end load. The proposed method leverages a control set of seven voltage vectors, each characterized by a zero ZSV component, effectively eliminating ZSV-related issues. To further enhance output current quality, three of these voltage vectors are applied during each sampling interval. Simulation results validate the superior performance of the proposed method, which is achieving a significant reduction in THD of the output current to 2.4%, compared to 6.2% and 45.5% achieved by conventional approaches. The

effectiveness of the topology and the proposed method have become a promising solution in transportation and industrial applications, especially in traction and actuation motor drives, where the elimination of ZSC is important.

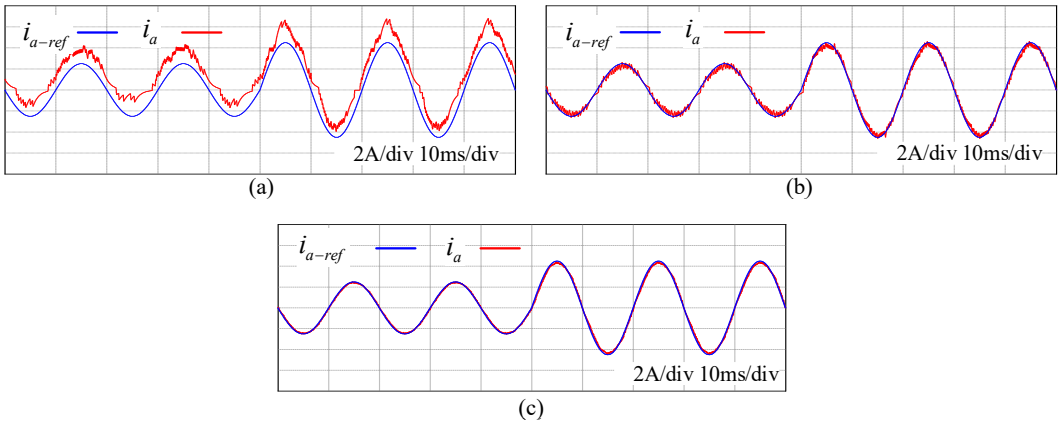

Figure 11. Dynamic response of a) Method I, b) Method II, and c) Method III

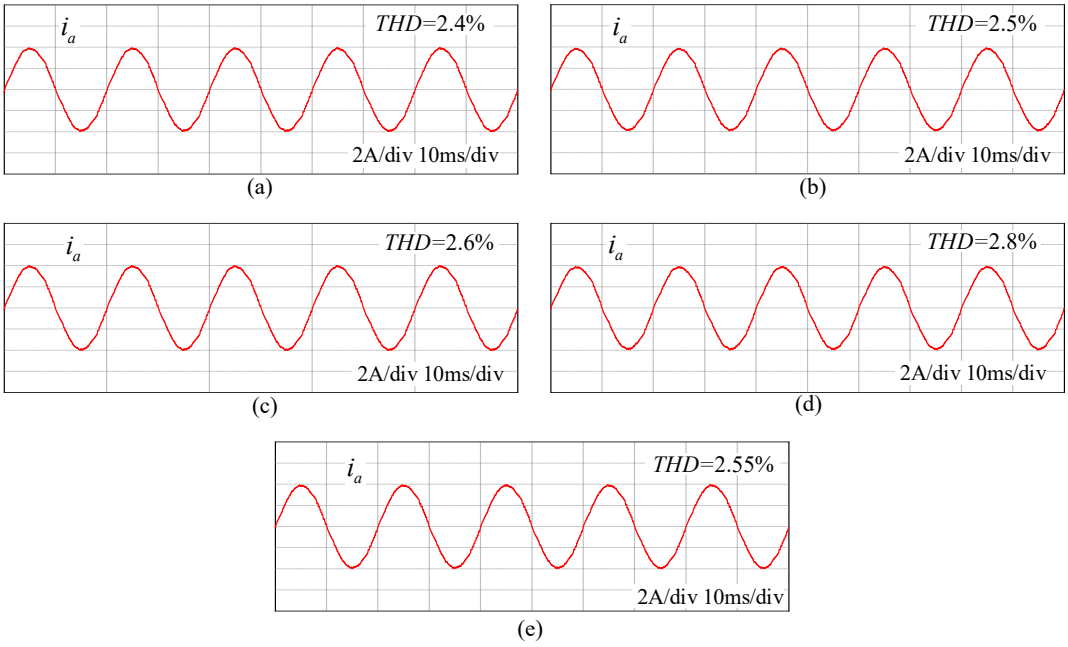

Figure 12. Output current THDs with the variation of load resistance R and inductance L.
(a) Accurate R and L, (b) 0.85R and accurate L, (c) 1.15R and accurate L,
(d) Accurate R and 0.85L, and (e) Accurate R and 1.15L.

REFERENCES

1. Trabelsi M., Vahedi H., and Abu-Rub H. - Review on single-DC-source multilevel inverters: Topologies, challenges, industrial applications, and recommendations, IEEE Open Journal of the Industrial Electronics Society **2** (2021) 112-127. https://doi.org/10.1109/OJIES.2021.3054666
2. Gupta K., Ranjan A., Bhatnagar P., Sahu L., and Jain S. - Multilevel Inverter Topologies with Reduced Device Count: A Review, IEEE Transactions on Power Electronics **31** (2016) 135-151. https://doi.org/10.1109/TPEL.2015.2405012

3. Munawar S., Iqbal M., Adnan M., Ali Akbar M., and Bermak A. - Multilevel inverters design, topologies, and applications: Research issues, current, and future directions, IEEE Access **12** (2024) 149320-149350. https://doi.org/10.1109/ACCESS.2024.3472752
4. Sarker R., Bhattacharya A., Debnath S., Castillo-Atoche A., and Datta A. - A Novel FPGA-Driven HD-SPWM Architecture with Zero-Sequence Voltage Insertion Strategy for Three-Level NPC Inverter, IEEE Trans. on Ind. Infor. **20** (2024) 10814-10824. https://doi.org/10.1109/TII.2024.3393566
5. Escalante M., Vannier J., and Arzande A. - Flying capacitor multilevel inverters and DTC motor drive applications, IEEE Trans. on Ind. Elect. **49** (2002) 809-815. https://doi.org/10.1109/TIE.2002.801231
6. Guo F., Ma Z., Diao F., Zhao Y. and Wheeler P. - Hybrid Virtual Coordinate-Driven CBPWM Strategy of Three-Level T-Type NPC Converters for Electric Aircraft Propulsion Applications, IEEE Trans. on Industrial Electronics **71** (2024) 2309-2319. https://doi.org/10.1109/TIE.2023.3266552
7. Chen M. and Sun D. - A unified space vector PWM for dual two-level inverter system, IEEE Trans. on Power Electronics **32** (2017) 889-893. https://doi.org/10.1109/TPEL.2016.2585223
8. Wang, Baoji, Xing Zhang, and Renxian Cao. - A zero-sequence steerable CBPWM strategy for eliminating zero-sequence current of dual-inverter fed open-end winding transformer-based PV grid-tied system with common DC bus, IEEE Access **8** (2020) 81220-81231. https://doi.org/10.1109/ACCESS.2020.2991135
9. Yu Z., Gan C., Ni K., Wang S., Liu X., Sun Jianbo, and Qu R. - Optimized nine-switch converter-fed flux-modulated doubly salient reluctance motor drive with integrated ZSC regulation ability considering efficiency improvement, IEEE Transactions on Transportation Electrification **10** (2024) 9281-9293. https://doi.org/10.1109/TTE.2024.3357860
10. Huu-Cong Vu, and H-H Lee - Simplified model predictive current control strategy for dual five-phase VSI-fed open end load to eliminate common-mode voltage and reduce current harmonics, Journal of Power Electronics **21** (2021) 1155-1165. https://doi.org/10.1007/s43236-021-00266-0
11. Gu W., Liao H., Lin J., Li Z. and Jin T. - Control strategy of three-level NPC inverter based on variable coefficient virtual vector model predictive control, IEEE Open Journal of Circuits and Systems **3** (2022) 288-297. https://doi.org/10.1109/OJCAS.2022.3218823
12. H. -C. Vu, Q. -H. Tran, D. -A. Dong, K. D. Hoang and T. L. Van - A simple MPCC to improve current performance with fixed switching frequency for four-leg VSI fed two-phase loads, 2023 Inter. Conf. on System Science and Engineering (ICSSE), Ho Chi Minh, Vietnam, 2023, pp. 358-362. https://doi.org/10.1109/ICSSE58758.2023.10227156
13. Jin N., Dai D., Xie H., Wu J. and Guo L. - Virtual vector-based FCS-MPC for NPC three-level grid-tied inverter without weighting factor of neutral-point voltage balancing, IEEE Access **10** (2022) 72806-72814. https://doi.org/10.1109/ACCESS.2022.3187994
14. Yang Y., Wen H., Fan M., Zhang X., He L., Chen R., Xie M., Norambuena M., and Rodriguez J. - Low complexity finite-control-set MPC based on discrete space vector modulation for T-type three-phase three-level converters, IEEE Transactions on Power Electronics **37** (2022) 392-403. https://doi.org/10.1109/TPEL.2021.3098661
15. Q. -B. Nguyen, P. C. Dung, H. -C. Vu, T. N. Dinh and Q. -H. Tran - A modulated model predictive control for three-phase three-level T-type inverter, 2022 11th Inter. Conf. on Control, Automation and Information Sciences (ICCAIS), Hanoi, Vietnam, 2022, pp. 190-195. https://doi.org/10.1109/ICCAIS56082.2022.9990390
16. Huu-Cong Vu and Hong-Hee Lee - Simple MPCC strategy for three level sparse five-phase VSI to suppress current harmonics with balanced neutral-point voltage, IEEE Transactions on Power Electronics **37** (2022) 771-781. https://doi.org/10.1109/TPEL.2021.3094193
17. Rodriguez J., Pontt J., Silva C. A., Correa P., Lezana P., Cortes P., and Ammann U. - Predictive current control of a voltage source inverter, IEEE Transactions on Industrial Electronics 54 (2007) 495-503. https://doi.org/10.1109/TIE.2006.888802

TÓM TẮT

PHƯƠNG PHÁP ĐIỀU KHIỂN DỰ BÁO DÒNG ĐIỆN ĐỂ ĐỒNG THỜI TRIỆT TIÊU THÀNH PHẦN ĐIỆN ÁP THỨ TỰ KHÔNG VÀ GIẢM SÓNG HÀI DÒNG ĐIỆN ĐẦU RA CHO BỘ NGHỊCH LƯU CHÍN KHÓA CẤP CHO TẢI MỞ

Vũ Hữu Công[1], Trần Quốc Hoàn[2]*

[1]*Trường Đại học Xây dựng Hà Nội,*

[2]*Trường Đại học Trần Đại Nghĩa*

*Email: *hoantq@tdnu.edu.vn*

Bài báo này đề xuất một phương pháp điều khiển dự báo dòng điện nhằm mục đích loại bỏ thành phần điện áp thứ tự không (ZSV) và giảm sóng hài dòng điện đầu ra cho bộ nghịch lưu chín khóa (NSI) cấp cho tải mở (open-end load). Phương pháp đề xuất sử dụng một tập đầu vào gồm bảy véc-tơ điện áp, mỗi véc-tơ triệt tiêu thành phần ZSV, để đảm bảo loại bỏ ZSV hoàn toàn. Đồng thời, ba véc-tơ điện áp trong số này được áp dụng trong mỗi chu kỳ lấy mẫu để cải thiện chất lượng dòng điện đầu ra. Kết quả mô phỏng trên phần mềm PSIM cho thấy phương pháp đề xuất không chỉ loại bỏ hiệu quả thành phần ZSV mà còn giảm đáng kể méo dạng sóng hài toàn phần (THD) của dòng điện đầu ra, chứng minh tiềm năng ứng dụng thực tiễn của phương pháp này.

Từ khóa: Điều khiển dự báo dòng điện, bộ nghịch lưu chín khóa, thành phần điện áp thứ tự không, giảm sóng hài dòng điện.